Original Article

A longitudinal ^{18}F-fluorodeoxyglucose (^{18}F-FDG) and ^{18}F-sodium fluoride (^{18}F-NaF) positron emission tomography/computed tomography (PET/CT) study in apolipoprotein E (ApoE) knockout rats fed with a Western diet

Xiaoqing Zhuang[1]^, Yue Feng[2], Juan Li[1], Feng Zhao[1], Yu Zhang[2], Yue Chen[2]

[1]Department of Nuclear Medicine, General Hospital of Ningxia Medical University, Yinchuan, China; [2]Department of Nuclear Medicine, Affiliated Hospital of Southwest Medical University, Luzhou, China

Contributions: (I) Conception and design: X Zhuang, Y Chen; (II) Administrative support: J Li, F Zhao; (III) Provision of study materials or patients: X Zhuang, Y Feng, Y Zhang; (IV) Collection and assembly of data: X Zhuang, Y Feng; (V) Data analysis and interpretation: X Zhuang; (VI) Manuscript writing: All authors; (VII) Final approval of manuscript: All authors.

Correspondence to: Xiaoqing Zhuang. Department of Nuclear Medicine, General Hospital of Ningxia Medical University, Yinchuan 750004, China. Email: zhuangxq@nyfy.com.cn; Yue Chen. Department of Nuclear Medicine, The Affiliated Hospital, Southwest Medical University, No. 25, Taiping St., Luzhou 646000, China. Email: chenyue5523@126.com.

Background: Inflammation and vascular calcification are risk factors for cardiovascular disease, but their relationship is still under investigation. This longitudinal *in vivo* study aimed to monitor inflammation and calcification during the formation of atherosclerotic plaques in apolipoprotein E knockout (ApoE$^{-/-}$) rats by ^{18}F-fluorodeoxyglucose (^{18}F-FDG) and ^{18}F-sodium fluoride (^{18}F-NaF) positron emission tomography/computed tomography (PET/CT).

Methods: In the ApoE group, male ApoE$^{-/-}$ rats were fed a high-fat Western diet from 13 weeks of age, and in the normal group, male SD rats of the same age were fed a normal diet. A longitudinal PET/CT study using ^{18}F-FDG and ^{18}F-NaF was performed at 12, 27, and 46 weeks of age. T1-weighted magnetic resonance imaging (MRI) was used as an atlas template, and the uptake of the tracers in the cardiovascular system was analyzed based on atlas 3D geometry volumes-of-interest (VOIs). After the PET/CT study, pathological and immunohistochemical examinations were performed on the corresponding lesions.

Results: The body weight and plasma cholesterol levels of the ApoE$^{-/-}$ rats increased with time, and at each time point, significantly higher body weight and plasma cholesterol levels were observed in the ApoE$^{-/-}$ rats than in the normal rats. PET/CT showed that in ApoE$^{-/-}$ rats, the uptake of ^{18}F-FDG was found in the aortic arch, while the uptake of ^{18}F-NaF was found in pulmonary arteries. The uptake of the two tracers in the ApoE group increased with time. Extensive early stage of atherosclerotic plaques, with high expression of CD68 and alizarin red, were observed in pulmonary arteries. However, only a thickened intima with very high expression of hypoxia-inducible factor-1 alpha (HIF-1α) was seen in the aortic arch.

Conclusions: In ApoE$^{-/-}$ rats fed a high-fat Western diet, early atherosclerotic lesions developed in the pulmonary arteries; however, ^{18}F-FDG failed to accumulate in these lesions but to accumulate in the aortic arch with only neointimal hyperplasia and significantly high expression of hypoxia.

Keywords: ApoE$^{-/-}$ rat; atherosclerosis; 18F-fluorodeoxyglucose positron emission tomography/computed tomography (^{18}F-FDG PET/CT); 18F-sodium fluoride positron emission tomography/computed tomography (^{18}F-NaF PET/CT); hypoxia

Submitted Jul 06, 2020. Accepted for publication Dec 23, 2020.
doi: 10.21037/cdt-20-609
View this article at: http://dx.doi.org/10.21037/cdt-20-609

^ ORCID: 0000-0001-8652-8540.

Introduction

Vascular inflammation and calcification occur as part of atherosclerosis. They are both actively controlled processes that play a key role in atherosclerosis. In human atherosclerosis, inflammation and calcification interweave with each other, and their relationship is unclear. Positron emission tomography/computed tomography (PET/CT) is a highly sensitive and noninvasive molecular imaging modality that offers the opportunity to explore a variety of pathophysiological processes within atherosclerotic plaques *in vivo* using various radiotracers.

^{18}F-fluorodeoxyglucose (^{18}F-FDG) is a radiolabeled glucose analog. It can be transported into cells by glucose transporters and phosphorylated by hexokinases, but it cannot be metabolized further and becomes trapped in cells (1). ^{18}F-FDG is a nonspecific radiotracer that is taken up by cells with an elevated metabolic rate and an increased number of glucose transporters compared to normal cells (2). In addition to malignant tumor cells, glucose transporters are also increased in active inflammatory cells, such as macrophages (3-5). Thus, ^{18}F-FDG, as a marker for active inflammation, is often used for the detection of atherosclerosis in preclinical and clinical studies.

^{18}F-sodium fluoride (^{18}F-NaF) is a tracer for active microcalcification. The mechanism is ^{18}F-fluoride ion exchange with hydroxyl groups on the surface of hydroxyapatite crystals, the dominant component of both bone and vascular calcifications (6-8). Unlike calcium scoring measured by CT, which quantifies established macrocalcifications, ^{18}F-NaF quantifies the current active microcalcification status (9-12).

The apolipoprotein E (ApoE) gene produces ApoE to participate in the transport of cholesterol-rich lipoproteins. Knockout of the ApoE gene results in high cholesterol levels in the blood and the development of atherosclerosis (13). Because the size of the rat can provide a more detailed image *in vivo* and the characteristics of lipid metabolism in rats are more similar to those of humans than the mouse model (14), the ApoE$^{-/-}$ rat model is becoming attractive in cardiovascular system PET/CT imaging. However, there are only a few studies on atherosclerosis in the ApoE$^{-/-}$ rat model.

This study aimed to track the development of vascular inflammation and calcification in an early stage of atherosclerosis by ^{18}F-FDG and ^{18}F-NaF PET/CT imaging using a high-fat Western diet ApoE$^{-/-}$ rat model. However, our results showed that ^{18}F-FDG PET imaging failed to visualize inflammation in early atherosclerotic lesions but instead might reveal hypoxia in the aortic arch.

We present the following article in accordance with the ARRIVE reporting checklist (available at http://dx.doi.org/10.21037/cdt-20-609).

Methods

Ethical approval for this original research was obtained from the General Hospital of Ningxia Medical University Animal Ethics Committee (2013-0301), in compliance with national or institutional guidelines for the care and use of animals.

Animals

A total of 23 rats were used in this study. For the ApoE group, 19 male ApoE$^{-/-}$ rats were purchased from Biocytogen (through TALEN technology; Beijing Biocytogen Co., Ltd., Beijing, China). As a control group, three male Sprague-Dawley (SD) rats were purchased from the experimental animal center in the Affiliated Hospital of Southwest Medical University. One male SD rat aged 12 weeks purchased from Southeast University was used for a magnetic resonance imaging (MRI) study. The rats of the control group and ApoE group arrived at 9 weeks of age. Normal SD rats were housed in 1 cage, and ApoE$^{-/-}$ rats were housed with 5 individuals per cage and a 12-h light interval at 21 ℃. ApoE$^{-/-}$ rats and SD rats were fed a normal diet (LAD1000M, Trophic Animal Feed High-tech Co., Ltd., China) after arrival. Then, the ApoE$^{-/-}$ rats were gradually changed to a Western-type diet (TP26305, Trophic Animal Feed High-tech Co., Ltd., China; 4.5 kilocalories/g, energy composition: 42% fat, 14% protein, 44% carbohydrate, 0.2% cholesterol) from 13 weeks of age. Diet and water were provided *ad libitum*. The rats were weighed at 12, 27, and 46 weeks of age before PET/CT scanning.

Cholesterol analysis

Blood samples were taken from the tail veins of the rats at 12, 27, and 46 weeks of age. Before blood sampling, rats have fasted for 12 h. Blood was collected in a heparin tube, and plasma was obtained by centrifugation of the blood at 3,000 rpm for 15 minutes at 4 ℃. Total cholesterol (TC), triglyceride (TG), low-density lipoprotein cholesterol (LDL-C), and high-density lipoprotein cholesterol

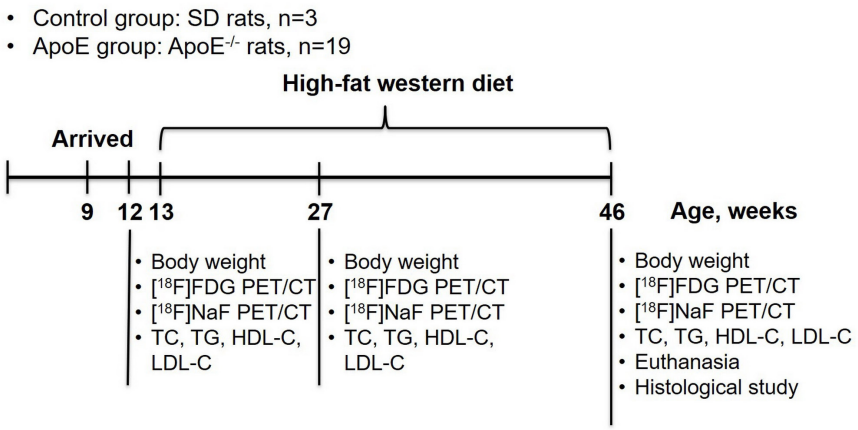

Figure 1 Schematic diagram of the study protocol. ApoE, apolipoprotein E; FDG, fluorodeoxyglucose; PET, positron emission tomography; CT, computed tomography; TC, total cholesterol; TG, triglyceride; HDL-C, high-density lipoprotein cholesterol; LDL-C, low-density lipoprotein cholesterol.

(HDL-C) levels were analyzed using an AU680 Automatic Biochemistry Analyzer (Beckman Coulter, USA).

Image protocol

The control group (n=3) and ApoE group (n=19) underwent PET/CT scans at 12, 27, 46 weeks of age using a PET/CT scanner (Inveon, Siemens, Munich, Germany). The study protocol is presented in *Figure 1*. The rats were fasted for 12 h before ^{18}F-FDG PET/CT scanning. Before scanning, the rats were anesthetized with 1–2% isoflurane, and ^{18}F-FDG (30.5±8.3 MBq) was injected intravenously through the tail vein. After CT scanning, PET images were acquired at 60 minutes after injection for 30 minutes of static scanning. ^{18}F-NaF PET/CT (31.2±6.6 MBq) was conducted 1 day after ^{18}F-FDG PET/CT scanning using the same scanning protocol.

For the MRI study, a rat was anesthetized with 1–2% isoflurane. The MRI data were collected on a 7T Bruker Biospin scanner (Bruker, Ettlingen, Germany). The T1-weighted images were acquired in a 2D acquisition type, repetition time (TR) 500 ms, echo time (TE) 10 ms, number of excitations 4, slice thickness 1 mm, and field of view 3.5×3.5 cm and stored in a 256×256 matrix.

Image analysis

The 3D geometric volumes-of-interest (VOIs) of the aortic arch and pulmonary arteries were drawn using MRI images by Inveon Research Workplace Image Analysis software (Siemens Medical Solutions) (*Figure 2*) and used as an atlas template for PET analysis.

The PET and CT images were manually co-registered with the MRI template and analyzed using Inveon Research Workplace Image Analysis software (*Figure 2*). The ^{18}F-FDG and ^{18}F-NaF uptake of the aortic arch and pulmonary arteries were respectively assessed based on the atlas VOIs drawn by MRI. In each VOI, the mean standardized uptake value (SUV_{mean}) and the maximum standardized uptake value (SUV_{max}) were automatically measured by the software.

Histological studies

ApoE$^{-/-}$ rats were euthanized by cardiac puncture at 46 weeks after PET/CT scanning. The aortic arch and pulmonary arteries were observed under a dissection microscope. The artic arch and left pulmonary artery were excised, fixed in 4% paraformaldehyde, and embedded in paraffin. Each section was cut into 4-μm-thick slices. Adjacent slices were subjected to hematoxylin and eosin (HE) staining for overall morphology, alizarin red (NovaUltra Alizarin Red Stain Kit, IW-3001, IHC World, USA) staining for calcium, immunohistochemical staining with a CD68 antibody (BA3638; Boster, Wuhan, China) for inflammation, and immunohistochemical staining with a hypoxia-inducible factor-1 alpha (HIF-1α) antibody (PA1-16601, Thermo Fisher Scientific, USA) for hypoxia. Images were acquired with an optical scanner for qualitative and quantitative analysis. The integrated optical density (IOD)

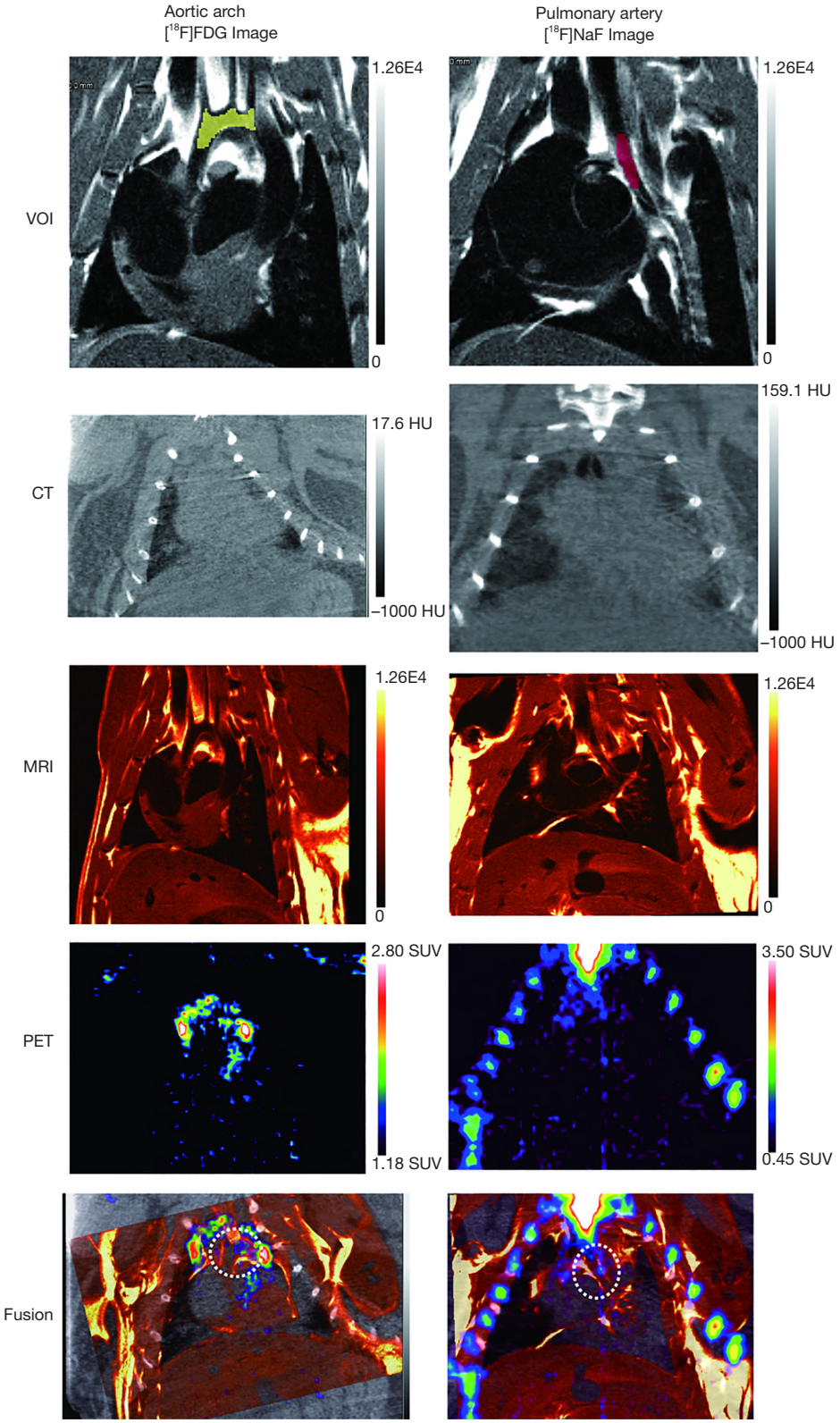

Figure 2 A representative example of atlas-based VOIs, CT, T1-weighted MRI, PET, and corresponding fusion images. VOIs, volumes-of-interest; CT, computed tomography; MRI, magnetic resonance imaging; PET, positron emission tomography; SUV, standardized uptake value.

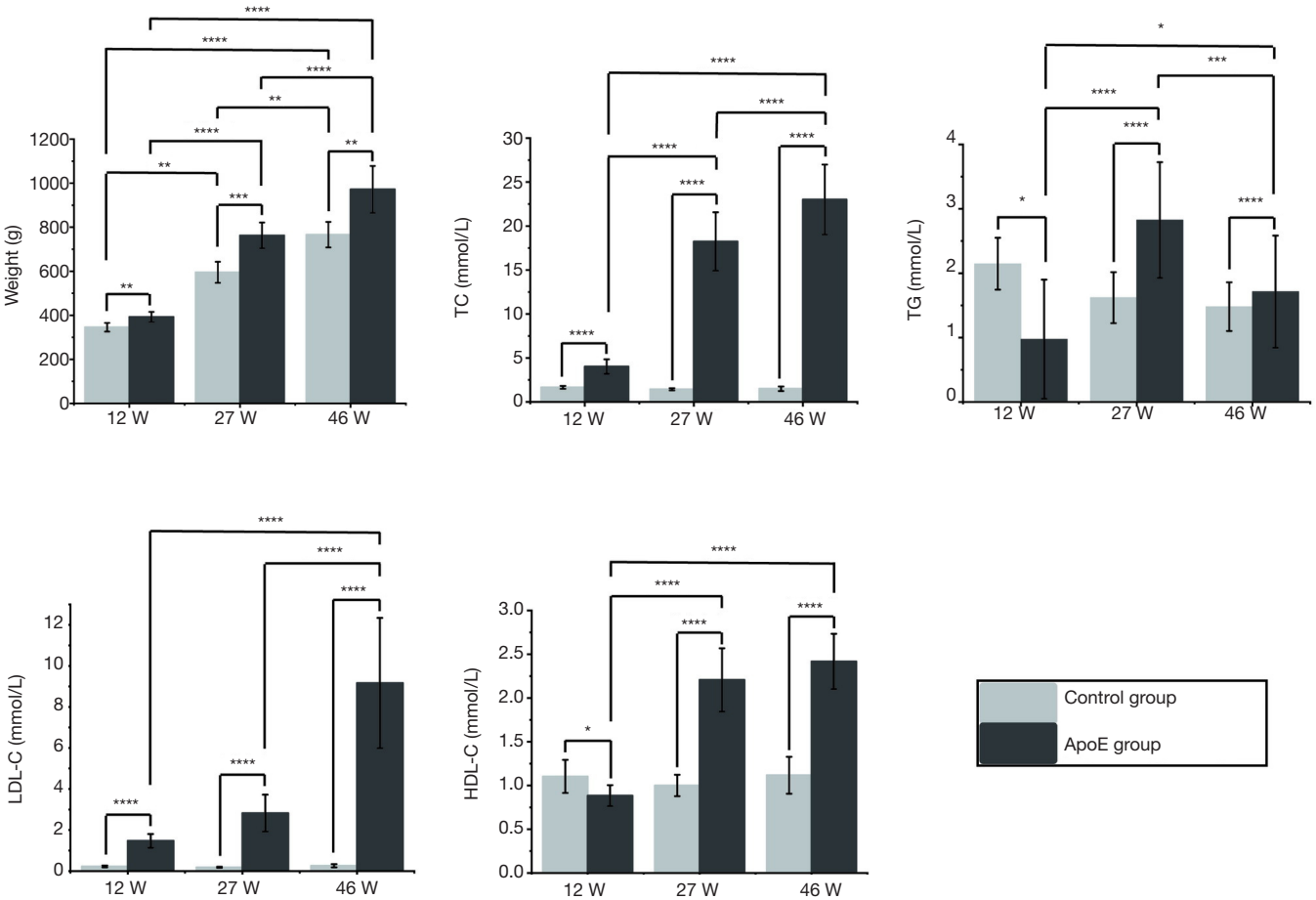

Figure 3 Body weight, plasma total cholesterol (TC), triglyceride (TG), low-density lipoprotein (LDL-C) cholesterol, and high-density lipoprotein (HDL-C) cholesterol levels of normal control rats (n=3) and ApoE$^{-/-}$ rats (n=19) at 12 weeks (12 W), 27 weeks (27 W) and 46 weeks (46 W) of age. The correlations between the groups were calculated by one-way ANOVA with a Tukey *post-hoc* test. *, P≤0.05; **, P≤0.01; ***, P≤0.001; ****, P≤0.0001.

and positive area of each component were assessed in each slice using ImageJ software (http://rsb.info.nih.gov/ij). The IOD value and the positive area of each section were determined by taking the average of these slices.

Statistical analysis

Data values are expressed as the mean ± standard deviation. Statistical analyses were performed using OriginPro 2018 software (Origin Lab Corporation, Northampton, MA, USA). The normality of the data distribution was tested by the Kolmogorov-Smirnov test. Differences between groups were analyzed using one-way analysis of variance (ANOVA) with a Tukey *post-hoc* test for normally distributed continuous data. For non-parametric data, data were analyzed by Kruskal-Wallis ANOVA with Dunn's *post-hoc* test. For all the tests, P<0.05 was considered to be statistically significant.

Results

Body weight gain and plasma cholesterol measurements

The body weight and plasma cholesterol data are shown in *Figure 3*. The body weights of ApoE$^{-/-}$ rats and control rats increased significantly with age (P<0.0001, n=19; P<0.0001, n=3, respectively). The TC, LDL-C and HDL-C levels in the ApoE group also increased with age (P<0.0001, P<0.0001, P<0.0001, respectively). At each time point, significantly higher body weight and plasma lipid levels

were observed in ApoE$^{-/-}$ rats than in control rats.

In vivo PET/CT imaging

^{18}F-FDG PET/CT and ^{18}F-NaF PET/CT images are presented in *Figures 2*,*4*. The PET/CT imaging results showed that in the cardiovascular system, ^{18}F-FDG accumulated in the aortic arch, while ^{18}F-NaF accumulated in either/both sides of the pulmonary arteries (*Figure 4A*).

The ^{18}F-FDG uptake in the aortic artery and ^{18}F-NaF uptake in both pulmonary arteries are shown in *Figure 4B,C*. In the control group, there was no significant correlation between ^{18}F-FDG and ^{18}F-NaF uptake with age (P>0.05 for all). In the ApoE group, the ^{18}F-FDG and ^{18}F-NaF uptakes were significantly correlated with age (P<0.0001 for all). No significant differences were observed in the ^{18}F-NaF uptake between the left pulmonary artery and right pulmonary artery at each time point (P>0.05 for all). At 46 weeks of age, the ^{18}F-FDG uptake in the ApoE group was significantly higher than that in the control group (P=0.011 for SUV_{mean}, P=0.014 for SUV_{max}). For both the left and right pulmonary arteries, the ^{18}F-NaF uptake in the ApoE group was significantly higher than that in the control group at 27 and 46 weeks of age (for the left pulmonary artery, at 27 weeks of age, P=0.0099 for SUV_{mean}, P=0.021 for SUV_{max}; at 46 weeks of age, P=0.011 for SUV_{mean}, P=0.011 for SUV_{max}; for the right pulmonary artery, at 27 weeks of age, P=0.017 for SUV_{mean}, P=0.012 for SUV_{max}; at 46 weeks of age, P=0.014 for SUV_{mean}, P=0.021 for SUV_{max}).

Histological studies

As shown in *Figure 5*, atherosclerotic lesions developed in the left and right pulmonary arteries of ApoE$^{-/-}$ rats. These lesions were at the early stage of atherosclerosis with fatty streaks. In the aortic arch of ApoE$^{-/-}$ rats, only neointimal hyperplasia was observed under a surgical microscope and on histological sections.

Immunohistochemical studies were performed on atherosclerotic lesions in the aortic arch and left pulmonary artery of both groups. Inflammation was measured with CD68 staining, calcification with alizarin red staining, and hypoxia with HIF-1α staining. In the control group, no significant difference was observed in the expression levels of CD68, alizarin red, and HIF-1α between the aortic arch and left pulmonary artery (P>0.05 for all, n=3). But for the ApoE group, the expression levels of CD68 and alizarin red in the left pulmonary artery were significantly higher than those in the aortic arch (P=0.001, n=17; P=0.013, n=17, respectively), while the expression level of HIF-1α in the left pulmonary artery was significantly lower than that in the aortic arch (P<0.0001, n=17). For the expression levels of alizarin red and HIF-1α in the aortic arch and CD68 and HIF-1α in the left pulmonary artery, the expression in the ApoE group was significantly higher than that in the control group (P=0.030; P=0.007; P=0.030; P=0.007, respectively).

Discussion

In this study, ^{18}F-FDG was used as a PET tracer to monitor inflammation in the formation of atherosclerosis in an ApoE$^{-/-}$ rat model. However, ^{18}F-FDG did not accumulate in atherosclerotic lesions with high expression of inflammation in pulmonary arteries.

ApoE$^{-/-}$ rats, generated through TALEN technology, were used as an atherosclerosis model to study the progression of atherosclerotic plaques. When fed a high-fat Western diet, the ApoE$^{-/-}$ rats developed dyslipidemia with excess body weights and high cholesterol levels. At the endpoint of this longitudinal study, 46 weeks of age (rats were fed a Western high-fat diet for 34 weeks), ApoE$^{-/-}$ rats developed extensive early stage of atherosclerotic plaques in the pulmonary arteries but only neointimal hyperplasia in the aortic arch. It is reported that ApoE$^{-/-}$ rats generated through TALEN technology were reported to be resistant to hyperlipidemia-induced endothelial inflammation (15), while ApoE$^{-/-}$ rats developed by the CRISPR/Cas9 technique could develop significant aortic plaques (16).

Atherosclerosis in pulmonary arteries has been reported in mice (17,18). This study is the first report describing pulmonary artery atherosclerosis in rats. We observed extensive plaques that developed in the pulmonary arteries, while atherosclerotic lesions in the aortic arch, as previously reported (15,19,20,21), were at the initial phase of atherosclerosis. As confirmed by surgical microscopy, H&E staining, CD68 staining, and alizarin red staining, atherosclerotic lesions in the pulmonary arteries were fatty streak lesions with larger areas of inflammation and calcification than those in the aortic arch. Intermittent hypoxia and hypercapnia are reported to induce pulmonary artery atherosclerosis in low density lipoprotein receptor deficient mice (22). For humans, pulmonary artery atherosclerosis is not common and related research is rather limited. Pulmonary hypertension is reported to be related to pulmonary artery atherosclerosis, but its relationship is

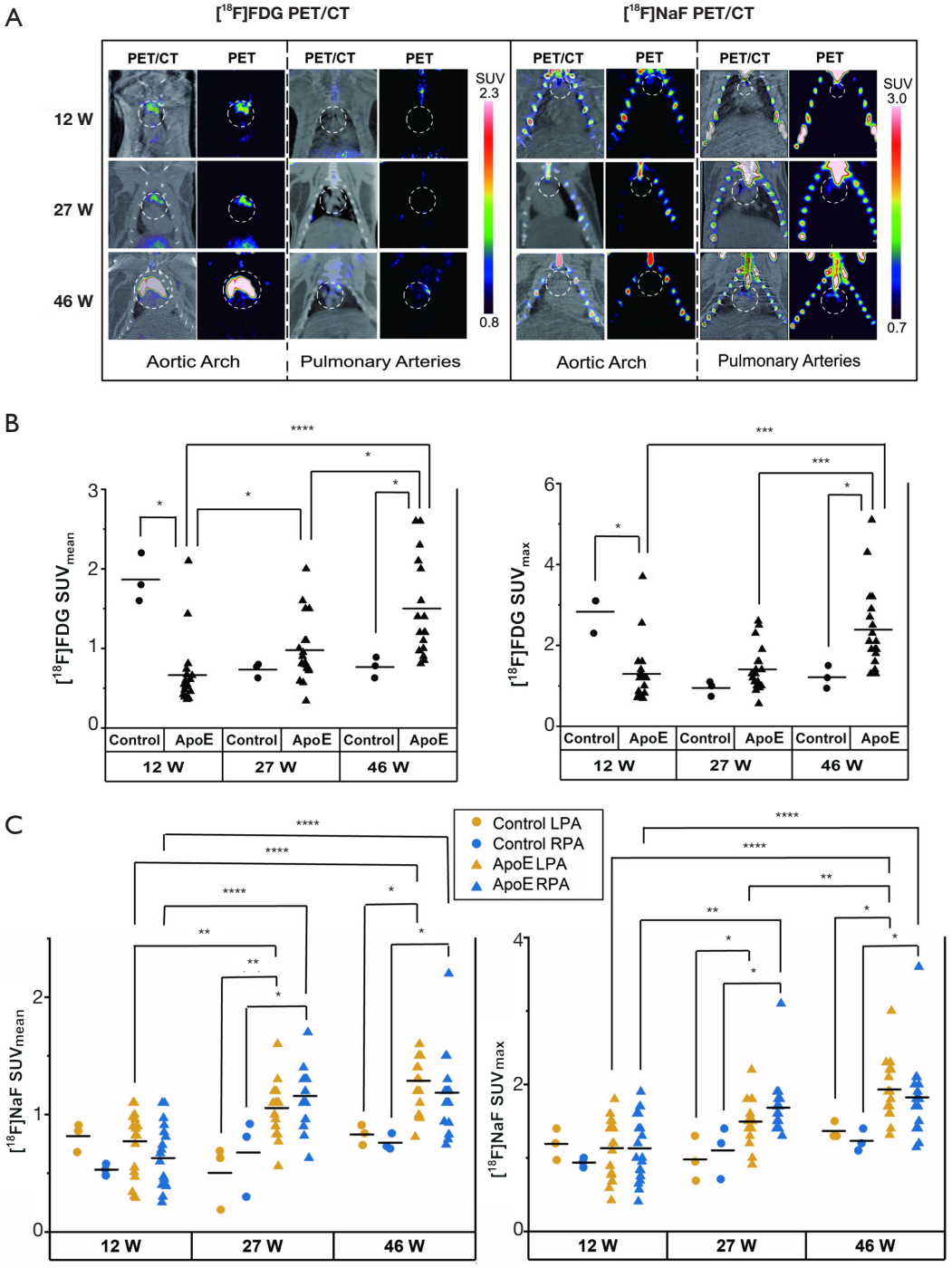

Figure 4 Representative PET/CT images of ^{18}F-FDG and ^{18}F-NaF around the aortic arch and pulmonary arteries in the ApoE group (n=19) (A). The exact locations of the aortic arch and pulmonary arteries were identified by the application of the atlas onto the co-registered PET/CT images. The uptake of ^{18}F-FDG in the aortic arch (B) and ^{18}F-NaF in pulmonary arteries were extracted from the atlas-based VOIs in the normal group (n=3) and the ApoE group (n=19). The correlations between the groups were calculated by Kruskal-Wallis ANOVA with Dunn's *post-hoc* test. 12 W, 12 weeks of age; 27 W, 27 weeks of age, 46 W, 46 weeks of age. *, P≤0.05; **, P≤0.01; ***, P≤0.001; ****, P≤0.0001. FDG, fluorodeoxyglucose; PET, positron emission tomography; CT, computed tomography; SUV, standardized uptake value; LPA, left pulmonary artery; RPA, right pulmonary artery; ApoE, apolipoprotein E; VOIs, volumes-of-interest.

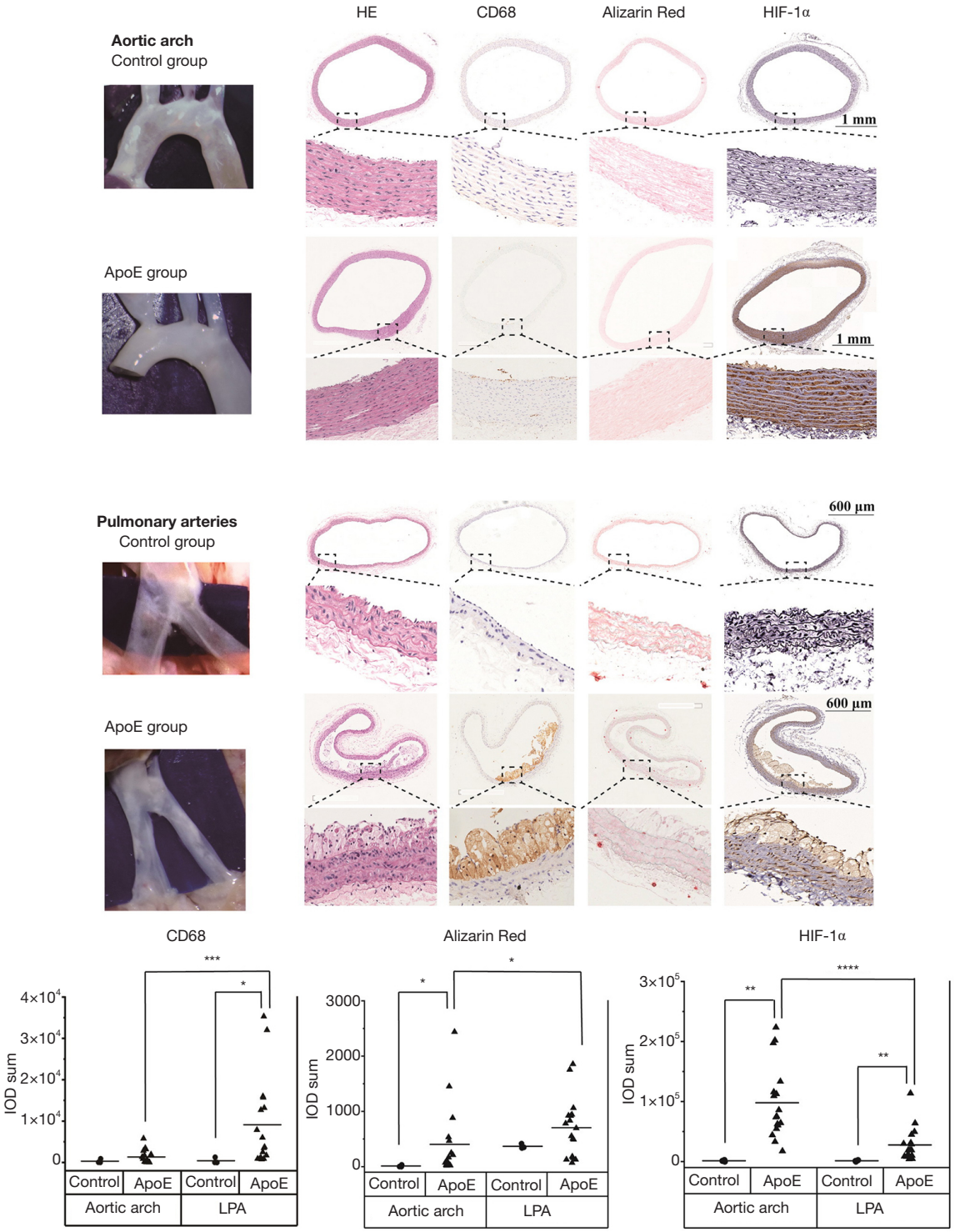

Figure 5 Pathology and immunohistological study of atherosclerotic lesions in the aortic arch and pulmonary arteries of the normal group (n=3) and the ApoE group (n=17). In the ApoE group, the expression of CD68 and alizarin red was significantly lower in the aortic arch than in the pulmonary arteries. However, the expression of HIF-1α in the aortic arch was significantly higher than that in the pulmonary arteries. The correlations between the groups were calculated by Kruskal-Wallis ANOVA with Dunn's *post-hoc* test. *, P≤0.05; **, P≤0.01; ***, P≤0.001; ****, P≤0.0001. LPA, left pulmonary artery; RPA, right pulmonary artery.

still unknown (23).

The availability of noninvasive imaging methodologies combining PET and CT provides the opportunity to understand the development and progression of atherosclerosis *in vivo*. ^{18}F-FDG and ^{18}F-NaF are two commonly used PET tracers that have already been used in clinical studies to investigate the mechanisms of atherosclerosis. ^{18}F-FDG was reported to accumulate in metabolically active macrophages and was widely used to detect active inflammation (3-5), while ^{18}F-NaF was used to identify active calcification (9-12). In this study, we monitored the formation of atherosclerotic plaques by using ^{18}F-FDG and ^{18}F-NaF PET/CT to visualize vascular inflammation and calcification. We assumed that ^{18}F-FDG, as an index of vascular inflammation, would first accumulate in the vasculature and that ^{18}F-NaF uptake, which is related to calcification, would appear at the same site later. However, in contrast to our prediction, although ^{18}F-FDG uptake did appear earlier than ^{18}F-NaF uptake, the two tracers were not present in the same arteries. ^{18}F-FDG accumulated in the aortic arch, while ^{18}F-NaF accumulated in the pulmonary arteries. CD68 staining showed that pulmonary arteries with higher inflammatory activity had no ^{18}F-FDG accumulation. Another study also reported that there was no ^{18}F-FDG accumulation in advanced atherosclerotic lesions of ApoE$^{-/-}$ mice (24). No correlation between ^{18}F-FDG uptake and CD68 expression levels in atherosclerosis studies was reported by Myers *et al.* (25). Hypoxia, rather than inflammation, has been suggested to cause ^{18}F-FDG accumulation (26). It has been reported that ^{18}F-FDG uptake is correlated with HIF-1α gene expression in human atherosclerotic carotid lesions (27-29). Therefore, in this study, HIF-1α staining was employed to identify hypoxia. The results indicated that the aortic arch with high ^{18}F-FDG uptake had significantly higher expression of hypoxia than pulmonary arteries with no ^{18}F-FDG uptake. Therefore, we proposed that ^{18}F-FDG reflects hypoxia rather than inflammation in early atherosclerotic lesions of ApoE$^{-/-}$ rats. The increase in ^{18}F-FDG uptake in the aortic arch with age reflects the increase in hypoxia during the process of atherogenesis. ^{18}F-NaF correlated well with microcalcifications in lesions and accumulated at more severe atherosclerotic lesions in the pulmonary arteries. ^{18}F-NaF PET/CT is a promising method to detect damage associated with vascular endothelial injury.

This study had some limitations. The spatial resolution of PET is not high enough to determine the exact location of the uptake of the tracer. Though we used atlas-based VOIs, the location of arteries may not be accurate enough. For example, the high ^{18}F-FDG uptake in the aortic arch of the control group at 12 weeks of age may be attributed to the spill-out effect of ^{18}F-FDG physiological uptake in the thymus gland (30). Autoradiography studies should be included in future studies. Although the accumulation of ^{18}F-FDG correlates with hypoxia rather than inflammation in rodent models, this may not be the case in humans. Further studies are needed. However, one should be very cautious in using the nonspecific PET tracer ^{18}F-FDG as an inflammation indicator in future studies.

Conclusions

Strikingly similar to the process of atherogenesis in humans, the ApoE$^{-/-}$ rat model provides a fertile source for the investigation of atherosclerotic plaques. In this study, we found that ApoE$^{-/-}$ rats fed a high-fat Western diet could develop early atherosclerotic lesions in the pulmonary arteries. However, ^{18}F-FDG accumulates in the aortic arch with high expression of hypoxia rather than inflammatory lesions in the pulmonary arteries. Thus, this longitudinal ^{18}F-FDG and ^{18}F-NaF PET/CT study showed the accumulation of hypoxia and microcalcifications at lesion sites *in vivo* during the process of atherogenesis.

Acknowledgments

The authors gratefully acknowledge Dan Zhao from the Radiology Department of Guangdong Hospital of Traditional Chinese Medicine for assistance with imaging analysis.

Funding: This work was supported by the National Natural Science Foundation of China (81360226).

Footnote

Reporting Checklist: The authors have completed the ARRIVE reporting checklist. Available at http://dx.doi.org/10.21037/cdt-20-609

Data Sharing Statement: Available at http://dx.doi.org/10.21037/cdt-20-609

Peer Review File: Available at http://dx.doi.org/10.21037/cdt-20-609

Conflicts of Interest: All authors have completed the ICMJE

uniform disclosure form (available at http://dx.doi.org/10.21037/cdt-20-609). The authors have no conflicts of interest to declare.

Ethical Statement: The authors are accountable for all aspects of the work in ensuring that questions related to the accuracy or integrity of any part of the work are appropriately investigated and resolved. Ethical approval for this original research was obtained from the General Hospital of Ningxia Medical University Animal Ethics Committee (2013-0301), in compliance with national or institutional guidelines for the care and use of animals.

References

1. Fowler JS, Ido T. Initial and subsequent approach for the synthesis of 18FDG. Semin Nucl Med 2002;32:6-12.
2. Pauwels EK, Ribeiro MJ, Stoot JH, et al. FDG accumulation and tumor biology. Nucl Med Biol 1998;25:317-22.
3. Yun M, Yeh D, Araujo LI, et al. F-18 FDG uptake in the large arteries: a new observation. Clin Nucl Med 2001;26:314-9.
4. Tawakol A, Migrino RQ, Bashian GG, et al. In vivo 18F-fluorodeoxyglucose positron emission tomography imaging provides a noninvasive measure of carotid plaque inflammation in patients. J Am Coll Cardiol 2006;48:1818-24.
5. Bucerius J, Dijkgraaf I, Mottaghy FM, et al. Target identification for the diagnosis and intervention of vulnerable atherosclerotic plaques beyond 18F-fluorodeoxyglucose positron emission tomography imaging: promising tracers on the horizon. Eur J Nucl Med Mol Imaging 2019;46:251-65.
6. Blau M, Ganatra R, Bender MA. 18 F-fluoride for bone imaging. Semin Nucl Med 1972;2:31-7.
7. Derlin T, Tóth Z, Papp L, et al. Correlation of inflammation assessed by 18F-FDG PET, active mineral deposition assessed by 18F-fluoride PET, and vascular calcification in atherosclerotic plaque: a dual-tracer PET/CT study. J Nucl Med 2011;52:1020-7.
8. Irkle A, Vesey AT, Lewis DY, et al. Identifying active vascular microcalcification by (18)F-sodium fluoride positron emission tomography. Nat Commun 2015;6:7495.
9. McEvoy JW, Blaha MJ, Defilippis AP, et al. Coronary artery calcium progression: an important clinical measurement? A review of published reports. J Am Coll Cardiol 2010;56:1613-22.
10. Derlin T, Richter U, Bannas P, et al. Feasibility of 18F-sodium fluoride PET/CT for imaging of atherosclerotic plaque. J Nucl Med 2010;51:862-5.
11. Dweck MR, Chow MW, Joshi NV, et al. Coronary arterial 18F-sodium fluoride uptake: a novel marker of plaque biology. J Am Coll Cardiol 2012;59:1539-48.
12. Joshi NV, Vesey AT, Williams MC, et al. 18F-fluoride positron emission tomography for identification of ruptured and high-risk coronary atherosclerotic plaques: a prospective clinical trial. Lancet 2014;383:705-13.
13. Moghadasian MH, McManus BM, Nguyen LB, et al: Pathophysiology of apolipoprotein E deficiency in mice: relevance to apo E-related disorders in humans. FASEB J 2001;15:2623-30.
14. Heinonen SE, Genové G, Bengtsson E, et al. Animal models of diabetic macrovascular complications: key players in the development of new therapeutic approaches. J Diabetes Res 2015;2015:404085.
15. Wei S, Zhang Y, Su L, et al. Apolipoprotein E-deficient rats develop atherosclerotic plaques in partially ligated carotid arteries. Atherosclerosis 2015;243:589-92.
16. Zhao Y, Yang Y, Xing R, et al. Hyperlipidemia induces typical atherosclerosis development in Ldlr and Apoe deficient rats. Atherosclerosis 2018;271:26-35.
17. Nakashima Y, Plump AS, Raines EW, Breslow JL, Ross R. ApoE-deficient mice develop lesions of all phases of atherosclerosis throughout the arterial tree. Arterioscler Thromb 1994;14:133-40.
18. Langheinrich AC, Michniewicz A, Bohle RM, et al. Vasa vasorum neovascularization and lesion distribution among different vascular beds in ApoE–/–/LDL–/– double knockout mice. Atherosclerosis 2007;191:73-81.
19. Ekuni D, Yoneda T, Endo Y, et al. Occlusal disharmony accelerates the initiation of atherosclerosis in ApoE knockout rats. Lipids Health Dis 2014;13:144.
20. Phillips EH, Chang MS, Gorman S, et al. Angiotensin II Infusion Does Not Cause Abdominal Aortic Aneurysms in Apolipoprotein E-Deficient Rats. J Vasc Res 2018;55:1-12.

21. Rune I, Rolin B, Lykkesfeldt J, et al. Long-term Western diet fed apolipoprotein E-deficient rats exhibit only modest early atherosclerotic characteristics. Sci Rep 2018;8:5416.
22. Douglas RM, Bowden K, Pattison J, et al. Intermittent hypoxia and hypercapnia induce pulmonary artery atherosclerosis and ventricular dysfunction in low density lipoprotein receptor deficient mice. J Appl Physiol 2013;115:1694-704.
23. Imamura T, Xue J, Poulsen O, et al. Intermittent hypoxia and hypercapnia induces inhibitor of nuclear factor-κB kinase subunit β-dependent atherosclerosis in pulmonary arteries. Am J Physiol Regul Integr Comp Physiol 2019;317:R763-9.
24. Laurberg JM, Olsen AK, Hansen SB, et al. Imaging of vulnerable atherosclerotic plaques with FDG-microPET: no FDG accumulation. Atherosclerosis 2007;192:275-82.
25. Myers KS, Rudd JH, Hailman EP, et al. Correlation between arterial FDG uptake and biomarkers in peripheral artery disease. JACC Cardiovasc Imaging 2012;5:38-45.
26. Folco EJ, Sheikine Y, Rocha VZ, et al. Hypoxia but not inflammation augments glucose uptake in human macrophages: Implications for imaging atherosclerosis with 18fluorine-labeled 2-deoxy-D-glucose positron emission tomography. J Am Coll Cardiol 2011;58:603-14.
27. Pedersen SF, Græbe M, Hag AM, et al. (18)F-FDG imaging of human atherosclerotic carotid plaques reflects gene expression of the key hypoxia marker HIF-1α. Am J Nucl Med Mol Imaging 2013;3:384-92.
28. Aarup A, Pedersen TX, Junker N, et al. Hypoxia-Inducible Factor-1α Expression in Macrophages Promotes Development of Atherosclerosis. Arterioscler Thromb Vasc Biol 2016;36:1782-90.
29. Yamashita A, Zhao Y, Matsuura Y, et al. Increased metabolite levels of glycolysis and pentose phosphate pathway in rabbit atherosclerotic arteries and hypoxic macrophage. PLoS One 2014;9:e86426.
30. Ferdinand B, Gupta P, Kramer EL. Spectrum of thymic uptake at 18F-FDG PET. Radiographics 2004;24:1611-6.

Cite this article as: Zhuang X, Feng Y, Li J, Zhao F, Zhang Y, Chen Y. A longitudinal ^{18}F-fluorodeoxyglucose (^{18}F-FDG) and ^{18}F-sodium fluoride (^{18}F-NaF) positron emission tomography/computed tomography (PET/CT) study in apolipoprotein E (ApoE) knockout rats fed with a Western diet. Cardiovasc Diagn Ther 2021;11(1):39-49. doi: 10.21037/cdt-20-609

